We are IntechOpen, the world's leading publisher of Open Access books Built by scientists, for scientists

6,900
Open access books available

185,000
International authors and editors

200M
Downloads

Our authors are among the

154
Countries delivered to

TOP 1%
most cited scientists

12.2%
Contributors from top 500 universities

WEB OF SCIENCE™

Selection of our books indexed in the Book Citation Index in Web of Science™ Core Collection (BKCI)

Interested in publishing with us?
Contact book.department@intechopen.com

Numbers displayed above are based on latest data collected.
For more information visit www.intechopen.com

23

Strontium Barium Niobate Thin Films for Dielectric and Electro-Optic Applications

Mireille Cuniot-Ponsard
Laboratoire Charles Fabry de l'Institut d'Optique, C.N.R.S., Univ Paris Sud
France

1. Introduction

The existence of strontium barium niobate crystals ($Sr_xBa_{1-x}Nb_2O_6$, noted SBN:100x) was first reported in 1960 (Francombe, 1960) and first large SBN single crystals were grown by Ballman and Brown over the range 0.25<x<0.75 (Ballman & Brown, 1966). In 1970, the Bell Telephone Laboratories had published successive thorough investigations of the optical, electrical, and structural properties of SBN crystals. The high values of the electro-optic and pyroelectric coefficients oriented further work mainly towards holographic and pyroelectric applications.

The development of SBN films started at the USSR Academy of Science in Novosibirsk (Baginsky et al., 1978) using a RF sputtering technique. Different deposition techniques have been then investigated: mainly sol-gel process, metal-organic chemical vapor deposition (MOCVD), and pulsed laser deposition (PLD).

Thin SBN films are particularly attractive for their potential use as low voltage electro-optic (e-o) waveguides. Electro-optic light modulation is a key function in light-wave technologies, mostly realized by exploiting the linear e-o Pockels effect in ferroelectric bulk crystals like lithium niobate (LN) for primary example. Optimizing the performance of an e-o modulator involves minimizing the half-wave voltage-length product ($V_\pi L$) and the drive power (P). A considerable decrease in the required $V_\pi L$ and P values, by three orders of magnitude, is expected from the replacement of bulk crystals by thin film waveguides about 1μm thick. Beside LN and SBN, the ferroelectric materials which have been considered in the literature in view of preparing electro-optic thin films are mainly $BaTiO_3$ (BT), $(Ba,Sr)TiO_3$ (BST), and $(Pb,La)(Zr,Ti)O_3$ (PLZT).

The implementation of Pockels e-o effect in thin film waveguides also opens up the path to the realization of electrically-tunable photonic crystal (PC) devices. Through the engineering of photonic band gaps, PC structures enable developing the functionality and reducing radically the size of optical devices. Theoretically position and shape of a photonic band gap can be electro-optically controlled. This e-o control considerably broadens the scope of PC structures potential functionality. The future deployment of photonic technology largely rests on the tunability of PC characteristics.

The Pockels electro-optic effect is the expression of the dielectric non linear properties in the range of optical frequencies where ionic displacement is negligible and relative dielectric permittivity is reduced to its electronic component. The interest for dielectric non linear

properties at lower frequencies, and particularly in the microwave region, has focused in the literature on another material (BST). This chapter devotes a significant part to the excellent dielectric non linear properties of SBN thin films. The great potential of SBN thin films is linked to our ability to control preparation and characterization. Through the successive sections, this chapter highlights some of the traps likely to deadlock research efforts.

2. Strontium barium niobate (SBN) crystals: main features

Strontium barium niobate ($Sr_xBa_{1-x}Nb_2O_6$, noted SBN : 100x) crystallizes in the region $0.25 < x < 0.75$ with the tetragonal tungsten bronze (TTB) structure represented in Figure 1 (Jamieson et al., 1968). The arrangement of NbO_6 octahedra in the form of five-members rings provides three types of interstitial sites: trigonal sites are vacant, tetragonal (A1) and pentagonal (A2) sites are partially occupied (5/ 6) by the divalent Sr and Ba atoms, and partially vacant (1/ 6) for reasons of electroneutrality. In this structure NbO_6 octahedra are not equivalent and two types must be distinguished. For both types the octahedral axes are not perfectly perpendicular to the (a, b) plane but slightly tilted from the polar c-axis (about 8°). Five formula units are necessary to form the unit cell depicted in the left part of Figure 1. Cell dimensions decrease with increasing the Sr/ Ba ratio due to the smaller atomic radius of Sr from {a=b ≈ 12.48 Å, c ≈ 3.98 Å} when x≈25% to {a=b ≈12.43 Å, c ≈ 3.91 Å} when x≈75% at room temperature. This double variation in lattice parameters and chemical composition modifies significantly the Curie temperature Tc of the ferroelectric crystal: Tc decreases from about 220°C when x≈25% to about 60°C when x≈75% (Ballman & Brown, 1967).

Above Tc the displacement of metallic atoms from their mean oxygen planes along the c-axis becomes zero except for one of the two types of Nb atoms (80% of them), which are distributed above and below oxygen planes with equal probability. The symmetry point group of the crystal transforms from *4mm* to $\bar{4}2m$, which is a non polar but also a non-centrosymmetric class. Birefringence and second harmonic generation exist above Tc.

SBN is a disordered crystal since each interstitial site A1 or A2 may be either occupied or vacant, and, if occupied, either by a Sr or a Ba atom. Local composition may change from cell to cell. As a result SBN is a ferroelectric relaxor exhibiting a broad phase transition.

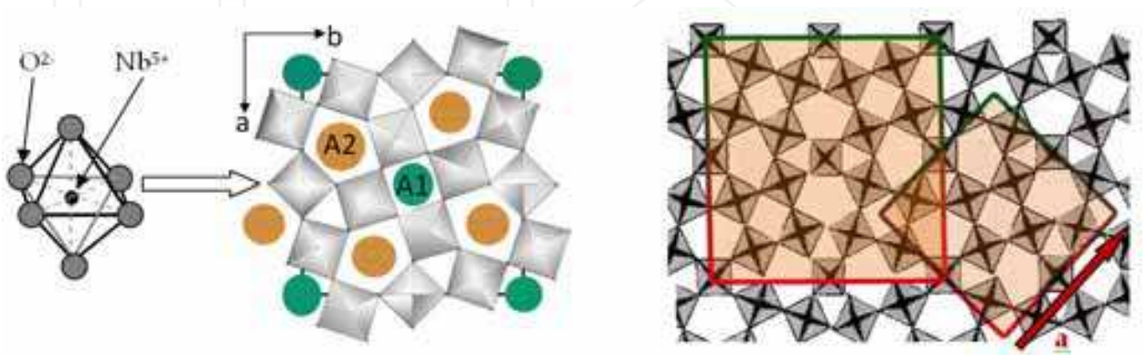

Fig. 1. View along the polar c-axis of the strontium barium niobate tetragonal tungsten bronze structure (After Jamieson et al., 1968). Rings made of five NbO_6 octahedra form three types of interstitial sites. The tetragonal (A1) and pentagonal (A2) positions are partially occupied by Sr and Ba atoms (5 / 6) and partially vacant (1/ 6).

SBN crystals are optically uniaxial negative ($n_e<n_o$) at room temperature. Compared to the ordinary index n_o in the (a, b) plane, the extraordinary index n_e along the polar c-axis is much more sensitive to both Sr content and temperature (Venturini et al., 1968). At λ=633 nm and room temperature, (n_o, n_e) vary from (2.314, 2.259) to (2.312, 2.299) when x varies from 25 to 75%, respectively. The domain of transparency is 0.35μm – 6 μm.
Ferroelectric, dielectric and non linear optic properties of SBN crystals are very sensitive to the Sr/ Ba ratio consistently with the impact of this ratio on Curie temperature (Glass, 1969; Lenzo, 1967). Increasing the Sr content reduces the interval between room and Curie temperatures, thus inducing a drastic enhancement of the dielectric permittivity, pyroelectric coefficient and non linear optic properties. Exceptionally large values of the linear electro-optic coefficient have been obtained (r_{33}=1340 pm/ V at λ=633 nm) with a 75% Sr content (Lenzo et al., 1967).

3. SBN thin films: preparation

3.1 Stoichiometry

The ternary phase diagram shown in Figure 2 (Carruthers & Grasso, 1970) indicates the different phases that may crystallize when mixing the three basic oxides SrO, BaO, and Nb_2O_5. The coloured field denotes the existence region of TTB SBN. The ternary solubility was found to extend from about 4% excess (Ba+Sr) to about 1% excess Nb_2O_5.

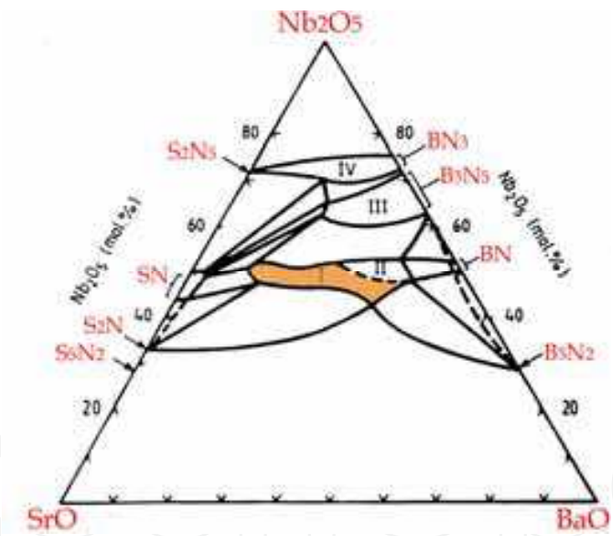

Fig. 2. Ternary phase relationships in the room temperature isotherm of the system BaO-SrO-Nb_2O_5, respectively denoted B-S-N in the chemical formula given along the axes. The coloured field is the existence region of the tetragonal tungsten bronze SBN phase (Carruthers & Grasso, 1970)

Stoichiometry of the deposit is a necessary but not sufficient condition for achieving single phase SBN thin films. Each deposition technique possesses its specific conditions for SBN stoichiometry, which must be established. In the case of the RF magnetron sputtering technique, the mechanisms which control the target-film composition transfer have been probed and their understanding exploited for stoichiometry control (Cuniot-Ponsard et al., 2003a). An illustration is given in Figure 3: two deposition parameters, the R.F. power and

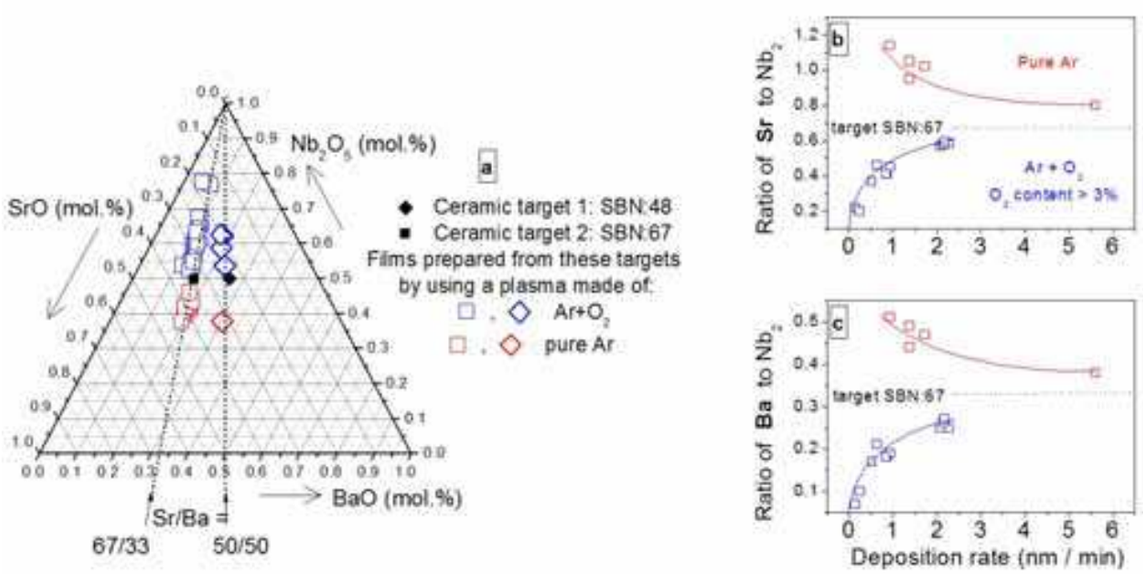

Fig. 3. (a) :Targets and sputtered films composition as determined from electron microprobe analysis. Differences in film composition have been obtained by varying R.F. power and oxygen percentage in the plasma. The other deposition parameters were fixed. (b) and (c) : Ratio of Sr and Ba to Nb_2, respectively, in films sputtered from a SBN:67 target as a function of deposition rate when this deposition rate is exclusively varied by modifying R.F. power. Oxygen percentage in the plasma is either zero (red symbols), or larger than 3% (3 to 15%) (blue symbols).

oxygen percentage in the plasma, have been varied and the resulting film composition is plotted in the ternary phase diagram. Targets and films composition has been determined by electron microprobe analysis using a single crystal of known composition (SBN: 60) as a standard. The film composition appears to be very sensitive to the varied parameters and large deviations from stoichiometry are observed. The presence of oxygen in the plasma changes the sign of the deviation: a lack of niobium becomes an excess niobium. This result indicates that the sputtering yield of niobium from the target is lower than that of the two other metallic atoms. On the other hand the Sr/ Ba ratio is mainly determined by the target composition and independent of deposition parameters, which suggests that divalent Sr and Ba atoms have similar properties in terms of both sputtering yield and reactivity with oxygen.

In both cases of non zero and zero oxygen percentages in the plasma, the opposite deviations from the target stoichiometry depicted in Figures 3b and 3c unambiguously decrease with increasing R.F. power. As might be expected, increasing R.F. power reduces the difference between Nb and (Sr, Ba) sputtering yields but it may be hazardous for the target integrity. Another way towards stoichiometry stands out in these figures, which consists in adjusting the oxygen percentage between 0 and 3%. Then the deposition rate can be chosen independently as low as desired. Stoichiometry is necessary to attempt to crystallise a SBN single phase and it is not usually spontaneous. It is often inferred from the observation of an X-ray diffraction spectrum consistent with that expected from SBN. The next section discusses this point.

3.2 Crystallization: the X-ray diffraction traps

The implementation of the Pockels e-o effect in SBN films requires (001) oriented films. Compared to the X-ray θ - 2θ patterns of polycrystalline SBN (Fig. 4), a (001) oriented SBN film is expected to display only the two peaks arrowed in the figure at $2\theta \approx 22.5°$ and 45.9°. In Figure 4 the powder X-ray spectrum calculated from the atom distribution model of Jamieson et al. is given for reference (Fig. 4a). As highlighted by vertical dashed lines (Fig. 4b-4c), an increase of the Sr content results in a slight shift of the SBN peaks towards higher 2θ values due to the decrease in lattice constants. The difficulty of preparing a single SBN phase increases with increasing the Sr/ Ba ratio close to the limit where the SBN phase becomes unstable (see Fig. 2). This explains the presence in the spectrum of the target SBN: 67 (Fig.4b) of parasitic peaks that issue from the phase $SrNb_2O_6$, noted SN in Fig. 2 (S for SrO and N for Nb_2O_5).

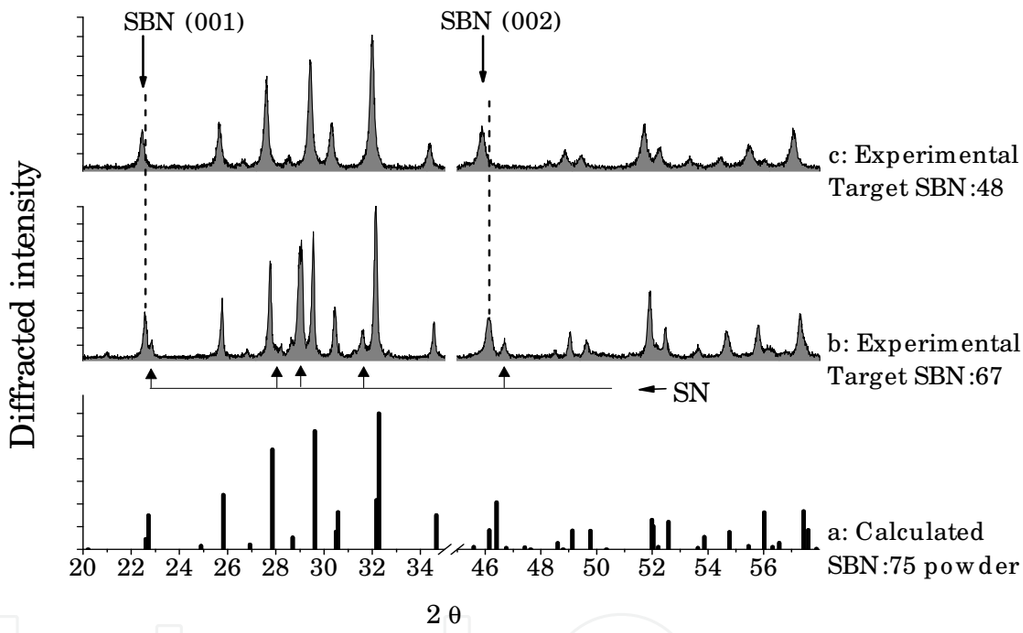

Fig. 4. X-ray θ - 2θ scan of a tungsten bronze SBN powder calculated from the atom distribution model for SBN : 75 (a) and experimental X-ray θ - 2θ scans measured from two polycrystalline targets SBN: 67 (b) and SBN: 48 (c). Target SBN: 67 is not single phase.

In the ternary phase diagram shown in Figure 2 some phases ($Sr_2Nb_{10}O_{27}$, $BaNb_2O_6$, $BaNb_6O_{16}$, $Ba_3Nb_{10}O_{28}$, respectively noted S_2N_5, BN, BN_3 and B_3N_5 in the diagram), have a c-cell parameter very close to that of the TTB SBN phase and consequently diffract their (001) and (002) peaks in very close angular locations as illustrated in Figure 5. Experimental data in the figure issue from the Joint Committee Powder Diffraction Standard - International Centre for Diffraction Data. The other cell parameters of these parasitic phases are also close to those (or to multiples) of the TTB SBN cell, so that the lattice-match and oriented (001) growth are similarly probable. Consequently, and taking into account the likely occurrence of a shift induced by epitaxial stress, the position of the (001) and (002) peaks in the X-ray

pattern of a (001) oriented film cannot be considered as a reliable signature of the TTB SBN phase. On the other hand, the ratio of the (001) to the (002) peak intensities provides an unambiguous means of distinguishing SBN from three of these four phases: S_2N_5 , BN_3 and B_3N_5. Phi-scan measurements are capable to rule out the remaining ambiguity.

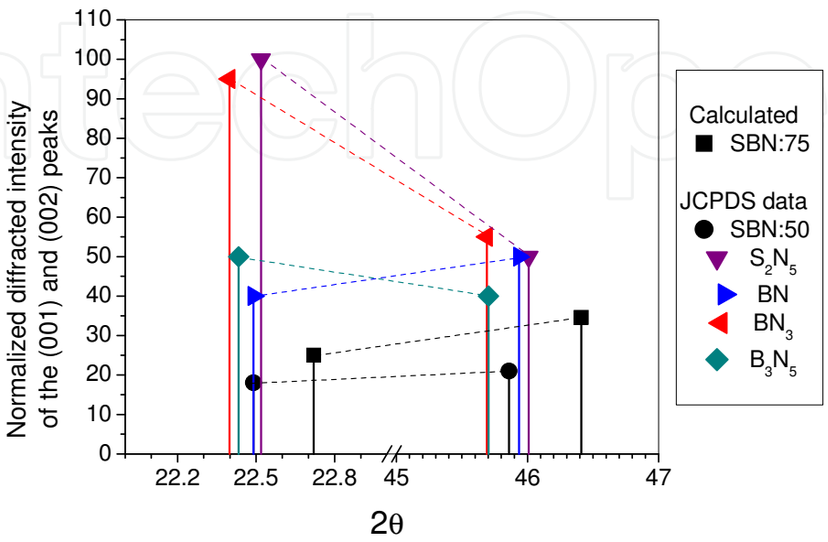

Fig. 5. Position and normalized diffracted intensity of the (001) and (002) peaks for the phases S_2N_5, BN, BN_3, B_3N_5, and SBN, from reported experimental data (Joint Committee Powder Diffraction Standard – JCPDS - International Centre for Diffraction Data), and calculated from the reported tetragonal tungsten bronze structure of SBN:75 (Jamieson et al., 1968)

3.3 Epitaxial crystallization on MgO and Pt covered MgO substrates

Magnesium oxide is the most common substrate used to grow epitaxial SBN thin films. Among the few substrate materials that can withstand temperatures higher than 700°C without reacting with the film, the reasons for choosing MgO are a small lattice mismatch (+1.2 to +1.6%, depending on Sr content, the positive sign implying a film tensile stress) and a large index contrast with SBN ($\Delta n = n_{SBN} - n_{MgO} \approx 0.5$ at $\lambda = 1.5$ µm). The oriented growth (001) SBN // (001) MgO has been reported from various deposition techniques including Metal Organic Chemical Vapor Deposition (MO-CVD) (Lu et al., 1994), Pulsed Laser Deposition (PLD) (Schwyn Thöny et al., 1994), Plasma Enhanced-CVD (Zhu et al., 1995), sol-gel synthesis (Sakamoto et al., 1996) and R.F. sputter deposition (Cuniot-Ponsard et al., 2003a). Figure 6 shows the X-ray diffraction spectrum of a (001) oriented SBN thin film prepared by RF magnetron sputtering of a ceramic target SBN: 60. The film was deposited amorphous then crystallized by using rapid thermal annealing. Rocking curves of the (001) and (002) peaks indicate a full width at half maximum of 0.65°.

When a bottom electrode is needed, a conductive crystalline substrate or a conductive epitaxial coating must be used. Among the possible conductive materials to be deposited on (001) MgO, platinum has been extensively studied for devices with ferroelectric, magneto-resistive, or magneto-optic applications, due to its chemical stability at high temperatures.

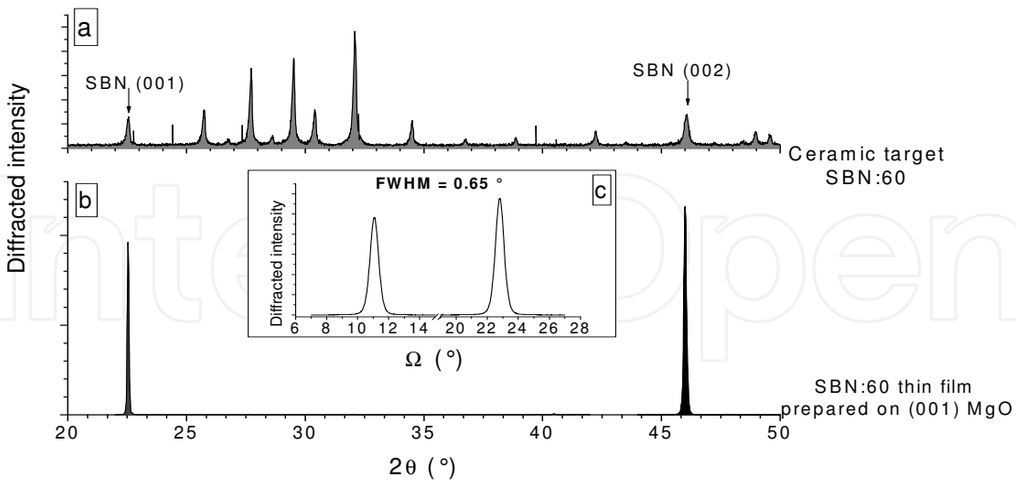

Fig. 6. (a) XRD θ - 2θ scan of a polycrystalline SBN:60 target as reference (b) XRD θ - 2θ scan of a film prepared from the previous target on a (001) MgO substrate by using the RF magnetron sputtering technique. (c) Rocking curves of the (001) and (002) peaks indicating a full width at half maximum of 0.65°.

Whatever deposition technique the authors used to prepare Pt thin films onto (001) MgO, the two orientations (111) and (001) were observed and found dominant at low and high deposition temperatures, respectively. However the reported temperature range in which the film orientation switches varies with the deposition technique: the lower the average energy of the depositing species, the higher the substrate temperature necessary to yield a dominant (001) Pt texture (Lairson et al., 1992; Narayan et al., 1994; McIntyre et al., 1995). This suggests that the incident kinetic and subsequent thermal energies of the depositing species are complementary regarding an energy threshold for the (001) Pt growth. The involvement of kinetic phenomena in the orientation development of the films has also been advanced. A decrease in the deposition rate has been reported (Ahn & Baik, 2002) to cause a drastic lowering of the orientation switching temperature (≈500°C→200°C). A similar lowering (≈500°C→350°C) can also be obtained with seeded substrates [Lairson et al., 1992). The epitaxial orientation relationship is of the type [110] Pt / / [110] MgO for both (001)Pt and (111)Pt crystallites on (001)MgO, which means cube–on-cube orientation for (001) Pt. Calculations have been carried out (MIntyre, 1997), which assign minima of the Pt/ (001)MgO interface energy to these two experimental in-plane alignments.
The (001) oriented growth of SBN onto Pt coated (001) MgO occurs exclusively on (001) oriented Pt crystallites (Cuniot-Ponsard et al., 2006). Figure 7 shows the X-ray symmetric patterns of two films simultaneously deposited and crystallized onto dominant (001) Pt and (111) Pt coatings, respectively. These spectra demonstrate a strong correlation between a (001) oriented SBN growth and the (001) orientation of underlying platinum. The integrated intensities of (001) SBN and (002) Pt reflections are found proportional: both are reduced to about 7% of their initial value from a spectrum (red) to the other (blue). Two other groups have published results about SBN thin films grown onto Pt coated MgO substrates [Sakamoto et al., 1996; Koo et al., 2000a]. Both prepared SBN by using a sol-gel process.

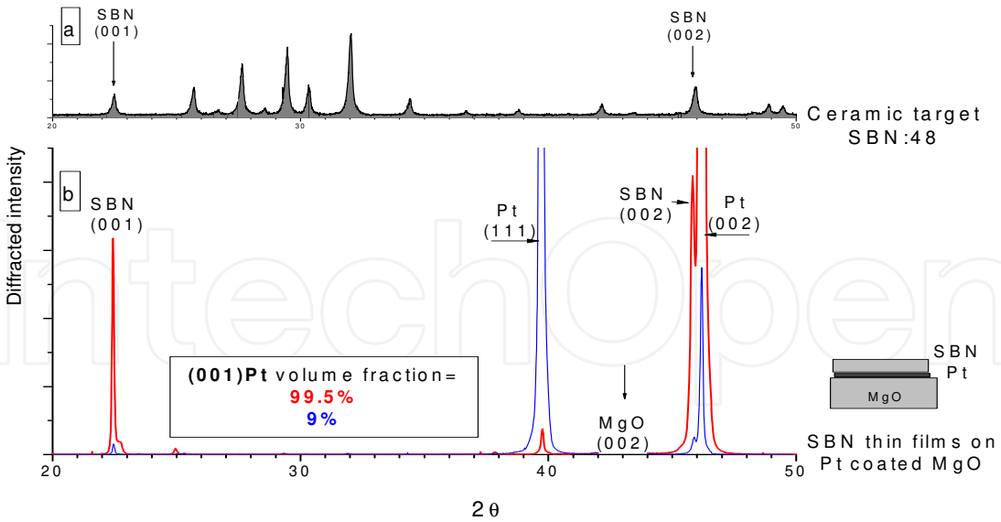

Fig. 7. Influence of the Pt crystallographic orientation on subsequent SBN growth: (a) XRD θ - 2θ scan of a polycrystalline SBN: 48 target as reference (b) XRD θ - 2θ scans of two films sputtered from the previous target, simultaneously deposited and crystallized on two Pt coated MgO (001) substrates only different in the (001) Pt volume fraction (99.5% and 9%).

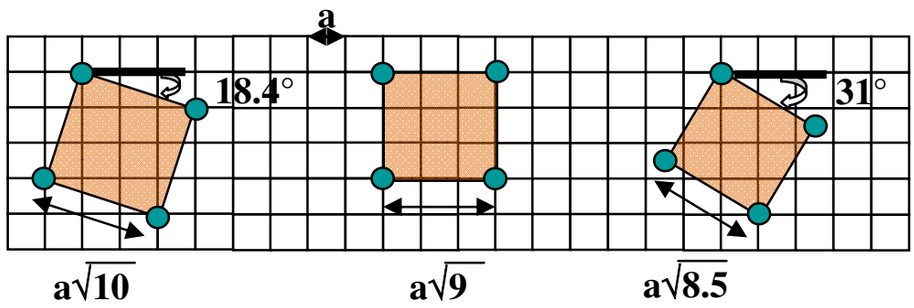

Fig. 8. Representation of the in-plane orientations experimentally observed for (001) SBN/ (001) MgO. The large lattice constant of crystalline SBN is between $a \times \sqrt{8.71}$ and $a \times \sqrt{8.78}$ depending on Sr content if a is the lattice constant of cubic MgO (a= 0.421 nm).

Despite the small lattice mismatch between SBN and MgO cell parameters in the film plane, aligned orientations have been rarely observed and were never dominant. For (001) SBN/ (001) MgO two couples of mirror symmetric in-plane orientations have been regularly reported in the literature since 1994 (Lu et al., 1994): ± 31° and ± 18.4° with respect to MgO cell axes (Fig. 8). The latter has been found present and dominant in all SBN thin films except in those we prepare by RF magnetron sputtering and in some samples prepared by RF plasma assisted Pulsed Laser Deposition (Scarisoreanu et al., 2008). This rotation by ± 18.4° implies a significant increase of the lattice misfit δ: $+1.2\% < \delta < +1.6\%$ (no rotation) becomes $+6.7\% < \delta < +7.1\%$ (for $25\% < x < 75\%$). An explanation involving the role of electrostatic energy across the interface has been proposed (Schwynn Thöny et al., 1994) and rejected (Willmott et al., 2005) in favour of another explanation based on the existence of a SN thin layer at the interface. On the contrary, a rotation by ± 31° changes the sign of the

lattice misfit but does not significantly modify its magnitude : +1.2%<δ<+1.6% (no rotation) becomes -1.6% <δ<-1.2% (for 25%<x<75%).

XRD phi-scans performed on SBN films prepared by sputtering demonstrate an epitaxial growth on both (001) MgO (Fig. 9a & b) and (001) Pt covered (001) MgO (Fig.9c & d). Two sets of planes, (211) and (311), have been selected on the basis of the high intensity they are expected to diffract at 2θ ≈ 27.7° and 32.1° respectively (see Fig.4). The only in-plane orientations which account for both (211) and (311) results are mirror symmetric (± α) to the MgO cell axes. The peaks location predicted from simulation for these two orientations is indicated in the figures with triangular symbols. As mentioned above, α is found equal to ± 31° for films deposited on MgO (Fig. 9a & 9b), which is consistent with a minimized lattice misfit. Among the parasitic phases likely to crystallize, SBN stoichiometry favours $SrNb_2O_6$ (SN), which grows epitaxially and (100) oriented on (001) MgO (Cuniot-Ponsard et al., 2003b). The presence of SN in the film prepared on MgO explains the parasitic peaks observed in the Φ scan. When the film is grown on (001) Pt / (001) MgO (Fig.9c & d), the SBN cell is found rotated by ± 18.4° with respect to the Pt and MgO cell axes. Contrary to the case discussed above of SBN/ MgO, and due to the lower lattice constant of the cubic Pt cell (a=0.391 nm), the orientation ± 18.4° corresponds to the minimized lattice misfit in the case SBN/ crystalline Pt (Fig. 8).

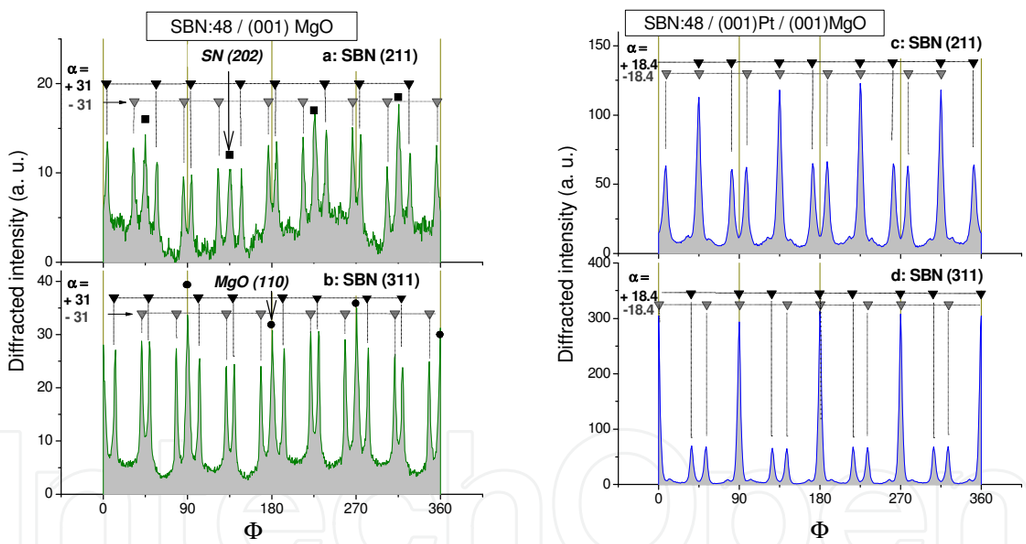

Fig. 9. Phi-scan measurements of the planes SBN(211), SBN(311) obtained from SBN: 48 thin films prepared by R.F. magnetron sputtering on (001) MgO (a,b) or (001) Pt / (001) MgO (c,d). The peaks location predicted from simulation for the two mirror symmetric in-plane orientations is denoted in the figures with triangular symbols. The presence of the parasitic phase $SrNb_2O_6$ (SN) in the film prepared on MgO is responsible for additional peaks assigned to SN (202) reflection.

A stoichiometric composition of the film is necessary but not sufficient to prevent the crystallisation of a mixture of parasitic phases like $SrNb_2O_6$ (SN) and $BaNb_2O_6$ (BN) of identical mean composition. The crystallization of a single phase SBN necessitates a minimum thermal energy whose amount increases when approaching the composition limits of SBN phase stability. An illustration is given in Figure 10 which compares the X-ray

diffraction patterns of two stoichiometric films prepared simultaneously by RF magnetron sputtering of a SBN: 60 target, then crystallized by rapid thermal annealing in identical conditions except the annealing duration. When the minimum thermal energy needed for SBN crystallization is not supplied (blue spectrum), a mixture of oriented SN and BN phases is obtained instead of a single phase SBN. Besides sufficient oxygen pressure during crystallization is necessary to prevent oxygen vacancies in the film structure. These oxygen vacancies are responsible for a strong loss of transparency in the near-infrared region (Fig.11a & b) and for large dielectric loss at low frequencies (Fig.11 c).

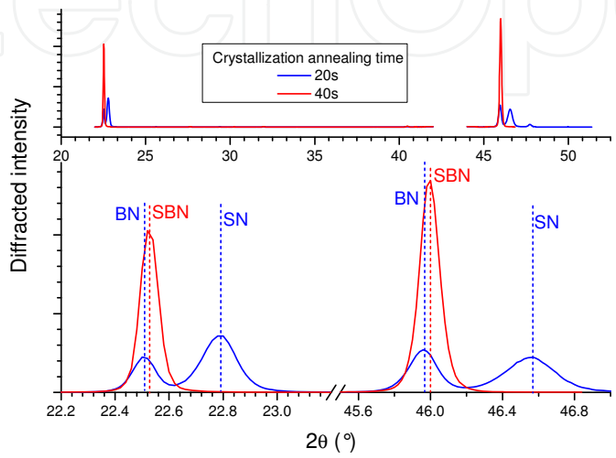

Fig. 10. X-ray diffraction spectra of two films prepared amorphous simultaneously by sputtering a SBN:60 ceramic target, then crystallized by rapid thermal annealing during either 20s or 40 s. A mixture of two parasitic phases $SrNb_2O_6$ (SN) and $BaNb_2O_6$ (BN) or a single phase SBN is obtained depending on the thermal energy supplied to the stoichiometric amorphous film.

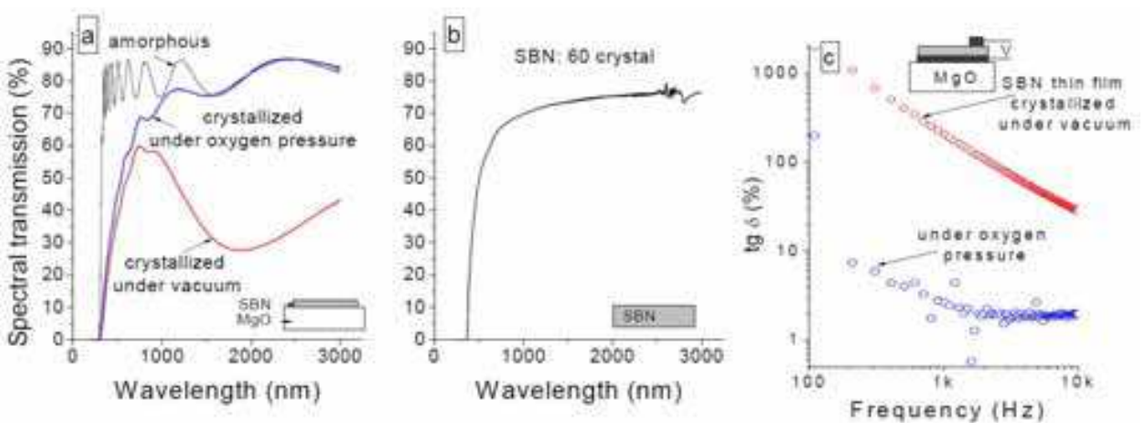

Fig. 11. Optical and electrical signatures of oxygen vacancies in SBN. (a) Optical transmission spectra of SBN films simultaneously prepared on MgO substrates and crystallized either under vacuum or oxygen pressure. The spectrum of the amorphous film before crystallization is also shown. (b) Optical transmission spectrum of a SBN: 60 crystal for reference. (c) Dielectric loss tangent versus frequency measured on Pt/ SBN/ Pt structures when SBN crystallization is achieved either under vacuum or oxygen pressure.

4. SBN thin films: dielectric properties

The dielectric properties of SBN crystals have been thoroughly investigated by Glass (Glass, 1969) as functions of temperature, frequency, dc electric field and Sr content. Concerning SBN thin films, the first detailed publication on ferroelectric properties (Antsigin, 1985) reported film properties similar to those of crystals. Such a complete similarity was not observed again until now. About fifteen papers have been published since, which report, often briefly, some dielectric properties of SBN films prepared by different techniques. The results vary strongly from a paper to another. Glass has shown that the dielectric permittivity deduced from the capacitance of a crystalline SBN disk sandwiched between two electrodes varied strongly with the nature of the electrodes, the specimen thickness and its degree of polarity. This influence of interfaces on the measured dielectric permittivity, necessarily enhanced in thin film measurements, is a first likely reason for the scattering of reported results. A second reason is to be found in the usual method used to record a Polarization-Electric field (P-E) hysteresis loop, which proceeds by integrating the current intensity induced by voltage variation in the circuit. The dielectric loss current is also integrated and may significantly contribute to form the observed hysteresis loop.

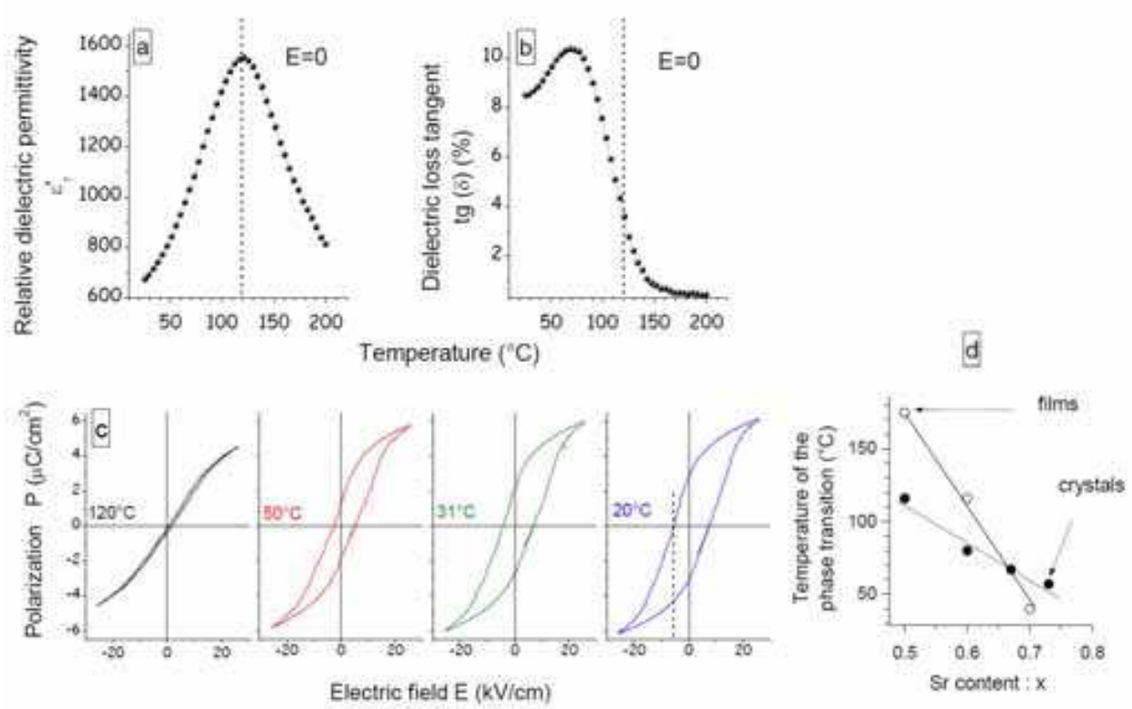

Fig. 12. Ferroelectric properties of a Pt / SBN / Pt structure prepared by sputtering from a SBN:0.60 target.(a-b) Zero field temperature dependence of the weak field relative dielectric permittivity and loss tangent at 10 kHz. (c) Polarization-electric field hysteresis loops recorded at a frequency of 33 Hz for different measurement temperatures. (d) Comparison of the phase transition temperature versus Sr content reported for crystals (Glass, 1969) and for epitaxial SBN films (Boulay, 2007).

Dielectric properties of epitaxial SBN thin films prepared by RF magnetron sputtering on (001) Pt covered (001) MgO substrates are presented in Figures 12, 13 & 14 (Boulay et al., 2007). Top platinum dots (0.5 and 0.3 mm in diameter) have been deposited by using R.F. magnetron sputtering. Capacitance and dielectric loss of the Pt / SBN / Pt sandwich structure are measured using a Hewlett Packard impedance analyzer. The weak field frequency is chosen equal to 10 kHz, which is high enough to eliminate the possible contribution of parasitic capacitances, and low enough to keep the effect of the measurement circuit inductance negligible. The polarization – field hysteresis loops are recorded at a frequency of 33 Hz using a Radiant Technologies RT66A analyzer.
A ferroelectric-paraelectric phase transition is observed in a temperature range depending on the Sr / Ba ratio (Fig. 12). The decrease of the transition temperature in the films with increasing Sr content is consistent with the evolution observed in crystals although it is of higher magnitude (Fig. 12d). As expected from a ferroelectric material, the shape of the polarization-electric field (P-E) loop becomes slimmer with increasing temperature and the hysteresis behaviour vanishes at the transition temperature(Fig.12c). The relative dielectric permittivity ε_r' and dielectric loss tangent ($tg\delta = \varepsilon''/\varepsilon'$, where ε' and ε'' are the real and imaginary parts of the dielectric permittivity) show a strong dependence on applied dc electric field (Fig.13). This field dependence varies with temperature similarly to the dielectric permittivity, and is maximum at the transition temperature. The electrical tunability of dielectric permittivity $\delta\varepsilon'/\varepsilon'\delta E$ is zero when electric field is equal to the coercive value, and maximum in the vicinity of this value. At room temperature the electrical tunability of SBN thin film dielectric permittivity is measured to be 1.8% cm/ kV for SBN: 60 and 1.6% cm/ kV for SBN: 67 (Fig. 14).

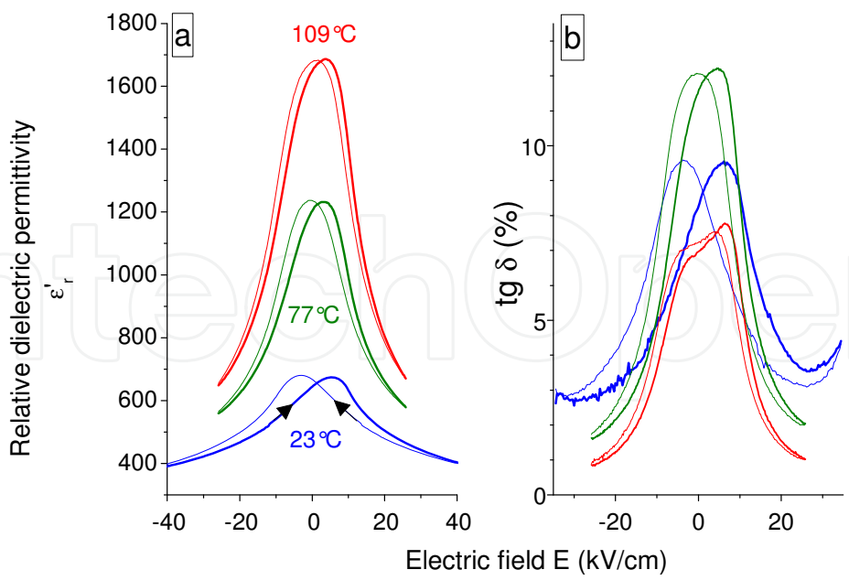

Fig. 13. Dielectric properties of a Pt / SBN / Pt structure prepared by sputtering from a SBN: 60 target. Electric field dependence of the weak field relative dielectric permittivity (a) and loss tangent (b) is measured at 10 kHz for different measurement temperatures.

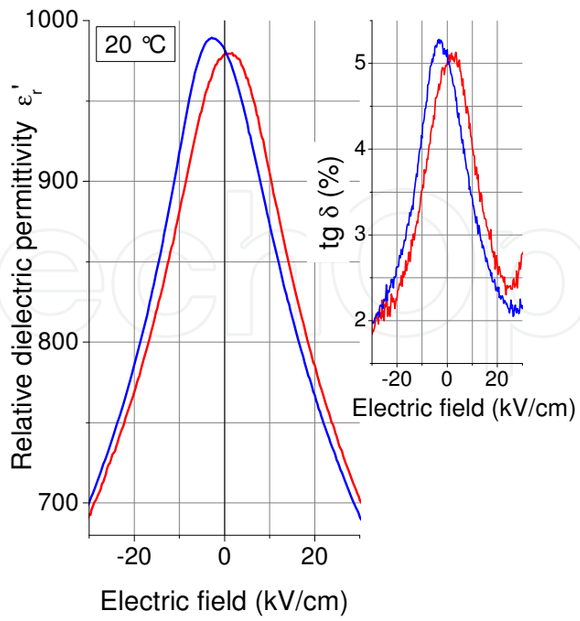

Fig. 14. Relative dielectric permittivity and loss tangent of a Pt / SBN / Pt structure prepared by sputtering from a SBN: 67 target, measured at 10 kHz and at room temperature. The electrical tunability of dielectric permittivity (δε'/ ε'δE) is 1.6% cm/ kV (16% μm/ V) at low dc electric field.

These values may be compared to that given by Glass for the electrical tunability of a SBN: 67 crystal (Glass, 1969) which is 4.4% cm/ kV. They should also be compared to the electrical tunability of (Ba, Sr)TiO_3 (BST) thin films which have been extensively investigated in view of exploiting this property in microwave applications. A value of 0.25% cm/ kV at low frequency (1MHz) was recently presented as an excellent result for BST thin films (Nozaka et al., 2008). The electrical tunability of SBN thin films prepared by PLD on MgO substrates has been measured by Moon et al. between 0.5 and 20 GHz and found to be 0.5% cm/ kV (Moon et al., 2004). The same authors compared phase shifters based on (Ba, Sr)TiO_3 and SBN thin films between 0.5 and 20 GHz, and concluded that these two materials were competitors for microwave tunable devices (Moon et al., 2005).

Some of the dielectric properties reported here are comparable with those reported by Liu et al. (Liu et al., 1995), Zhao et al. (Zhao et al., 2004), and Guerra et al. (Guerra et al., 2008) for SBN thin films prepared by using other techniques.

The values measured for the transition temperature, the dielectric permittivity and the coercive field, are consistent with the values reported for crystals. On the contrary the values measured for the polarization and the electrical tunability are about 5 times and 3 times lower, respectively, than those reported for crystals of similar composition. The dielectric tunability, as well as the electro-optic effect, involves the derivative $\delta^2P/\delta E^2$, where P and E are polarization and electric field. They are therefore expected to be (E,P)-dependent, and a correlated drop of polarization and electrical tunability is not surprising. Several possible reasons exist for a polarization lower in films than in crystals. They are presently under investigation.

5. SBN thin films: electro-optic properties

In this section, the dielectric permittivity is investigated at optical frequencies where ionic displacement is negligible and relative dielectric permittivity is reduced to its electronic component $\varepsilon_r = n^2$ (n is the complex index refractive of SBN).The electrical tunability of dielectric permittivity in this frequency range is the electro-optic (e-o) effect. It may be expressed in terms of an electric-field-induced distortion of the refractive index ellipsoid as:

$$\Delta(\frac{1}{n_{ij}^2}) = \sum_k r_{ijk} E_k \tag{1}$$

where n, r, and E represent, respectively, refractive index, electro-optic coefficient, and electric field. Only the first order terms (Pockels effect) have been kept in (1). The exceptionally high e-o coefficient in SBN is r_{33} (using reduced notation for r_{333}). A method enabling a reliable measurement of this coefficient in thin films is presented and applied to SBN films prepared by sputtering on (001)Pt/ (001)MgO substrates (Cuniot-Ponsard et al., 2011).

5.1 Usual experimental methods and difficulties

Methods used to determine the electro-optic coefficients of a thin film may be classified in three types: interferometric, polarimetric, and prism-coupling methods. In interferometric methods, an interference pattern is created with light beams, at least one of which propagates inside the e-o film. The electric-field-induced response of the e-o film causes a variation in phase and amplitude of the wave emerging from the film, and results in a variation (ΔI) in pattern light intensity. The different e-o coefficients are determined independently from the measurement of ΔI, by varying the direction of the linear polarization. In polarimetric methods the electric field induces a change ($\Delta\varphi$) in the relative phase between the two orthogonal components of a linearly polarized light beam. In most cases $\Delta\varphi$ is converted into an output light intensity variation ΔI by using an analyzer. From the measurement of $\Delta\varphi$ or ΔI, an "effective" e-o coefficient is determined, which is a linear combination of two e-o coefficients. Polarimetric methods do not enable the value of each e-o coefficient to be determined separately. In the prism-coupling technique (also called ATR for Attenuated Total Reflection) the film is sandwiched between two electrodes and forms a waveguide in which light is coupled by using a prism. The electric-field-induced response of the film modifies coupling incident angles, thus causing a variation ΔI in the intensity of the light beam emerging from the prism.

In all cases, the determination of e-o coefficients is carried out from measurement of the variation ΔI induced in output light intensity. The electric-field-induced response being a priori a combination of electro-optic, converse piezoelectric and electro-absorptive effects, the induced output signal ΔI is a function of the variations in refractive index (Δn_{ij}), in dimensions (Δe_i), and in extinction coefficients (Δk_{ij}), which may be expressed as:

$$\Delta I = \sum_{i,j} \frac{\partial I}{\partial n_{ij}} \Delta n_{ij} + \sum_i \frac{\partial I}{\partial e_i} \Delta e_i + \sum_{i,j} \frac{\partial I}{\partial k_{ij}} \Delta k_{ij} \tag{2}$$

Two sources of potential error affect the determination of e-o coefficients. The first is the use of approximations in view of simplifying the above expression (2): they consist in neglecting

optical effects like multiple reflections, and/ or some of the electric-field-induced effects like converse-piezoelectricity and electro-absorption. The further analysis of SBN films electric–field-induced response demonstrates the significant errors that can be induced by such approximations. The second source of potential error is the extreme sensitivity of derivatives appearing in (2) to a variation in the values of physical parameters of the films interacting with light (active film and electrodes). An illustration of this sensitivity is given in Figure 15. The example of a Fabry-Perot interferometric set-up has been chosen. The output reflected intensity I and the derivative $\partial I/\partial n_o$ (n_o is the ordinary refractive index of the active film) have been rigorously calculated for the transverse electric polarization TE without using any simplifying approximation. Figure 15 shows the plots of $\partial I/\partial n_o$ versus angle of incidence θ calculated from two sets of parameters with a small change only in the active film thickness value (e = 0.686 or 0.690 µm). The comparison between the two plots shows that if the actual thickness value is 0.686 µm instead of a believed value of 0.690 µm, this relative error of about +0.6% in one parameter value can induce a dramatic error in the value of the derivative $\partial I/\partial n_o$. Indeed the true value of the derivative will be multiplied by (-1) if measurement is performed at θ ≈ 31°, and by (1/ 3) if measurement is performed at θ ≈ 34°. Values of Δn_o and of the corresponding e-o coefficient will consequently be inferred erroneous in the inverse proportions, that is, obtained with the wrong sign if measurement is performed at θ ≈ 31°, or overestimated by a factor 3 if measurement is performed at θ ≈ 34°. From this simple demonstration it appears that determination of e-o coefficients is liable to drastic errors and must be necessarily checked independent of angle of incidence.

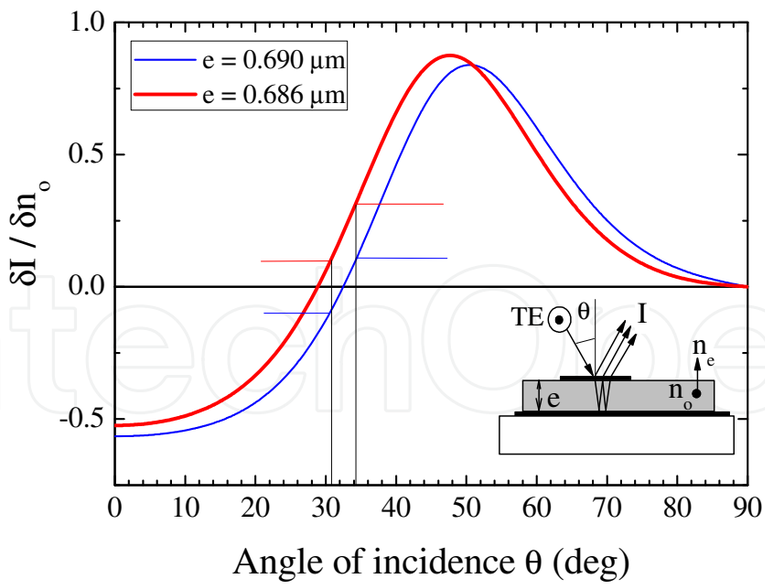

Fig. 15. Example of evolution of the derivative $\partial I/\partial n_o$ when slightly modifying one parameter, here the electro-optic film thickness value e, in a Fabry-Perot interferometric set-up. A variation in film thickness of only +0.6% (e = 0.686 →0.690 µm) can strongly modify the calculated derivative value: $\partial I/\partial n_o$ is multiplied by (-1) if measurement is performed at θ≈31°, and by (1/ 3) if measurement is performed at θ≈34°.

5.2 Principle of a reliable characterization method

The method exploits interferences obtained by reflection on the stack made of the e-o film sandwiched between two electrodes (Fig. 16). Reflectivity (R), and variation in reflectivity (ΔR) induced by an ac modulating voltage, are recorded versus incident angle θ, successively for TE and TM polarizations. According to the above expression (2):

$$\Delta R_{TE,\theta} = \left(\frac{\partial R}{\partial n_o}\right)_{TE,\theta} \Delta n_o + \left(\frac{\partial R}{\partial e}\right)_{TE,\theta} \Delta e + \left(\frac{\partial R}{\partial k_o}\right)_{TE,\theta} \Delta k_o \quad (3)$$

where Δe, Δn_o, Δk_o are the electric-field-induced variations of, respectively, the active film thickness e, its ordinary refractive index n_o, its ordinary extinction coefficient k_o.

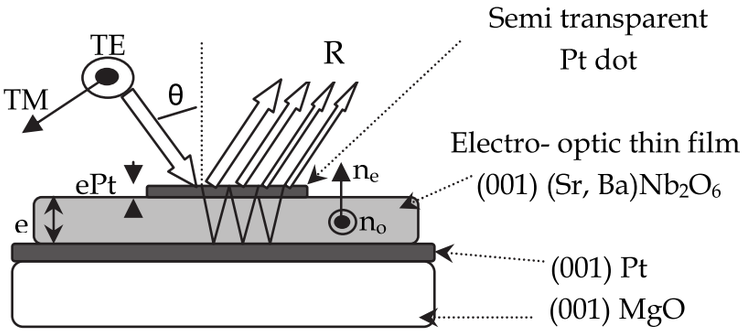

Fig. 16. Fabry-Perot interferometric configuration. Reflectivity (R), and variation in reflectivity (ΔR) induced by an ac modulating voltage, are recorded versus incident angle θ, successively for transverse electric TE and transverse magnetic TM polarizations

The calculation of reflectivity R is performed from Fresnel formulae by taking into account all the multireflection effects in the stack. The value of each derivative is numerically calculated. The determination of the three unknowns Δn_o, Δe, Δk_o appearing in (3) is then achieved by selecting three experimental data [$\Delta R_{TE}(\theta_1)$, $\Delta R_{TE}(\theta_2)$, $\Delta R_{TE}(\theta_3)$] and solving the inferred system of three linear equations. At this step, the e-o coefficient r_{13} and the converse-piezoelectric coefficient d_{33} can be deduced:

$$r_{13} = \frac{-2\, e\, \Delta n_o}{n_o^3\, \Delta V} \quad (4)$$

$$d_{33} = \frac{\Delta e}{\Delta V} \quad (5)$$

where ΔV is the ac modulating voltage amplitude. The refractive index of the film seen by TM polarization (n_θ) and its variation under electric field (Δn_θ) are dependent on θ, which prevents the use of a similar procedure. If θ_F represents the refracting angle of the light wave in SBN, n_θ and Δn_θ verify:

$$\frac{1}{n_\theta^2} = \frac{\cos^2\theta_F}{n_o^2} + \frac{\sin^2\theta_F}{n_e^2} \quad (6)$$

$$n_\theta = n_o \times \left(1 - \sin^2\theta \times \left(\frac{1}{n_e^2} - \frac{1}{n_o^2} \right) \right)^{1/2} \tag{7}$$

$$\Delta n_\theta = -\frac{n_\theta^3 \, \Delta V}{2\, e} \times \left(r_{13} \cos^2\theta_F + r_{33} \sin^2\theta_F \right) \tag{8}$$

According to (2):

$$\Delta R_{TM,\theta} = \left(\frac{\partial R}{\partial n_\theta} \right)_{TM,\theta} \Delta n_\theta + \left(\frac{\partial R}{\partial e} \right)_{TM,\theta} \Delta e + \left(\frac{\partial R}{\partial k_\theta} \right)_{TM,\theta} \Delta k_\theta \tag{9}$$

Derivatives appearing in (9) are calculated numerically like they were calculated for TE polarization except that dependence of index on θ must be taken into account. A value of incident angle is selected for which $(\partial R/\partial k_\theta)_{TM,\theta} = 0$, and equation (9) becomes a linear equation with a single unknown (Δn_θ). The e-o coefficient r_{33} is deduced from the solution Δn_θ through above expression (8).

From values of r_{13}, d_{33}, Δk_o, the electric-field induced response $\Delta R_{TE}(\theta)$ may be calculated versus incident angle and compared to the experimental data. For TM polarization, calculation of $R_{TM}(\theta)$ and $\Delta R_{TM}(\theta)$ versus incident angle may be carried out by considering n_e as a parameter. Calculation must be checked to account for the whole of experimental data : $R_{TE}(\theta)$, $R_{TM}(\theta)$, $\Delta R_{TE}(\theta)$ and $\Delta R_{TM}(\theta)$.

5.3 Electric-field induced response of SBN thin films

The previous procedure was carried out using a He-Ne laser radiation (λ=633 nm) and applied to the determination of SBN: 60 film coefficients. It yields the results indicated below (10).

$$\begin{aligned} r_{13} &= +8.5 \pm 1.3 \; pm/V \\ d_{33} &= \Delta e / \Delta V = +21 \pm 4 \; pm/V \\ \Delta k_o / \Delta V &= (+9.8 \pm 0.6) \times 10^{-6} \\ r_{33} &= +38.9 \pm 0.5 \; pm/V \\ r_{33}/r_{13} &= +4.5 \pm 0.6 \end{aligned} \tag{10}$$

Electro-optic, converse-piezoelectric and electro-absorptive components calculated from (10) are shown in Fig. 17 and Fig. 18 for TE an TM polarizations, respectively. As may be noticed, none of the three contributions is negligible and any attempt to account for experimental data without considering all of them would have been necessarily doomed to failure. Due to the opposite signs of Δn_o and Δe, phase shifts induced by electro-optic and converse-piezoelectric effects partially compensate one another so that the sum of these two contributions does not prevail over the electro-absorptive component in the final signal $\Delta R_{TE,\theta}$. A similar compensation is to be expected in a waveguide configuration if similarly low modulating frequencies are used. Measurements are therefore performed in unclamped conditions and the elasto-optic effect is likely responsible for a part of the measured coefficients. At high frequencies above piezo-electric resonance which are used in

information optical processing, the converse-piezoelectric effect is clamped and cannot counteract the electro-optic performance by inducing phase shift compensation as in the present measurements.

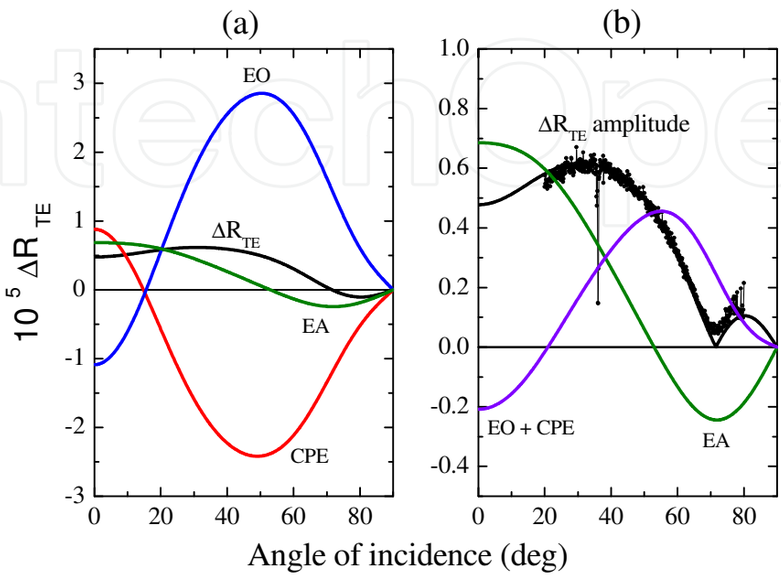

Fig. 17. (a) Electro-optic (EO), converse-piezoelectric (CPE) and electro-absorptive (EA) components of the electric-field induced variation in TE reflectivity (ΔR_{TE}) calculated from characterization procedure results. (b) Comparison between calculated (black continuous line) and experimental (black dots) ΔR_{TE} amplitudes. Amplitude of modulated voltage applied to SBN film is 1V. The plot of (EO+CPE) and (EA) components underlines the significant contribution of electro-absorptive effect to total TE response.

Figure 18 shows that the agreement between experimental and calculated data may be improved by varying the single adjustable parameter of this calculation: n_e. The resulting value of n_e ($n_e = n_o - 0.04$) is consistent with the birefringence value reported in the literature for crystalline SBN of similar composition at λ=633 nm ($n_e \approx n_o - 0.03$).

A few groups performed measurements of r_{33} in their SBN films. They reported r_{33} = 350 pm/ V (Trivedi et al.,1996), r_{33} = 173.4 pm/ V (Koo et al.,2000b), and r_{33} = 186 pm/ V (Li et al.,2008) for SBN:60 films. Multiple reflections in the film, converse-piezoelectric and electro-absorptive effects were neglected in the quoted reports and the authors did not control that results were consistent when varying incident angle. The e-o coefficient values previously reported for SBN films in the literature may be suspected of error for various reasons and would need to be confirmed.

Concerning SBN crystals, very few reports exist in the literature on the separate measurements of r_{13} and r_{33} in SBN crystals. At λ=633 nm and for a composition SBN:60, e-o coefficients have been determined separately in one paper (Zhang et al., 1991) which reports: r_{13}=37 pm/ V and r_{33}=237 pm/ V from measurements that do not enable specifying signs. On the other hand, the converse-piezoelectric coefficient d_{33} in SBN crystals was reported to be about 95 pm/ V. Compared to their crystalline counterpart, the three

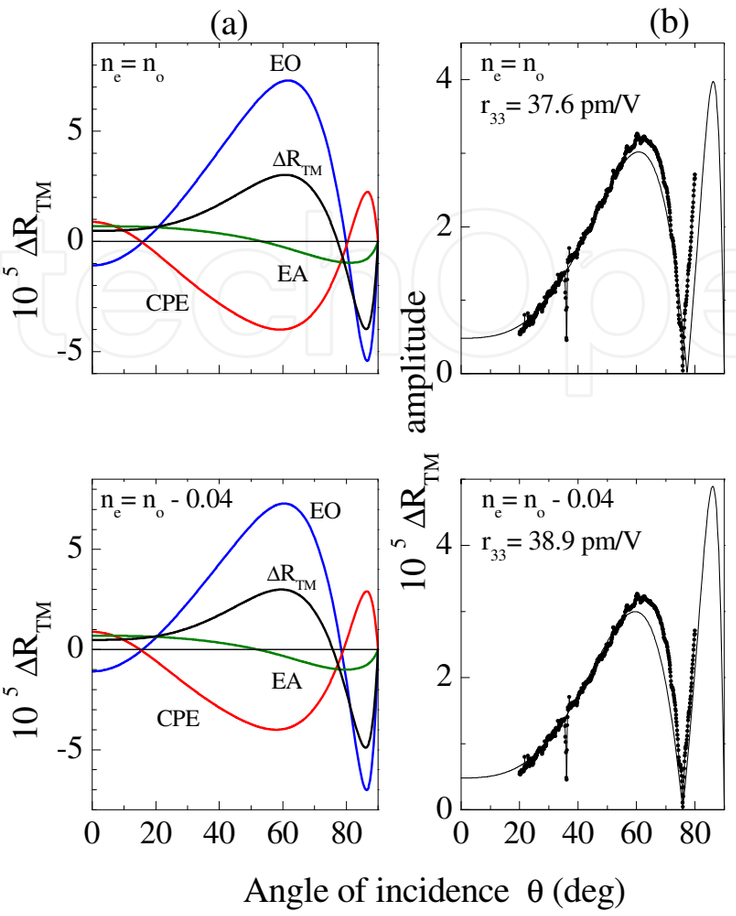

Fig. 18. Electric-field induced response for TM polarization (ΔR_{TM}). The three electro-optic (EO), converse-piezoelectric (CPE) and electro-absorptive (EA) contributions are detailed in (a) and comparison with experimental response is given in (b). Amplitude of modulated voltage applied to SBN film is 1V. Extraordinary refractive index n_e is the single adjustable parameter of characterization procedure; two cases are shown: $n_e = n_o$ (top) and $n_e = n_o - 0.04$ (bottom). The latter corresponds to the best calculation-experiment fit. The electro-optic coefficient r_{33} determined from characterization procedure and used for ΔR_{TM} calculation is equal to +37.6 (top) and +38.9 pm/ V (bottom).

coefficients r_{13}, r_{33}, d_{33} of the film appear reduced in similar proportions by a factor about 5±1. The magnitude of polarization in our SBN films is also measured about 5 times lower than that reported for SBN:60 single domain crystals. As already mentioned above, a correlation between these results is not surprising.

Although lower than those of SBN crystals, the application relevant e-o coefficients measured on SBN: 60 thin films (r_{33} = +38.9 pm/ V , $r_{eff} = r_{33} - (n_o/ n_e)^3 r_{13}$ = +29.9 pm/ V) are larger than those of a crystal of lithium niobate at the same wavelength λ=633 nm (r_{33} = +30.9 pm/ V, r_{eff} = +20.1 pm/ V). A further improvement of these SBN film coefficients is expected from the understanding of a lower polarization in films and from an increase in Sr content. The SBN thin film path is therefore proved to be competitive with regard to e-o modulation. Beside the e-o coefficient, the refractive index and the dielectric permittivity of

the material are also involved in the e-o performance. The low dielectric permittivity of lithium niobate is an advantage to be taken into account when comparing thin film paths.

6. Conclusion

An overview of the questions relative to the preparation, dielectric and electro-optic properties of strontium barium niobate thin films has been proposed, with a special focus on epitaxial growth in view of electro-optic applications. Results obtained with films prepared by RF magnetron sputtering have been presented.

The polarization, dielectric tunability at low frequency and electro-optic coefficients of epitaxial SBN thin films prepared on (001)Pt/ (001)MgO are found lower than those of crystals of the same composition in similar proportions. This correlation is not surprising and an understanding of the lower polarization in films should indicate the way towards a further improvement of the desired properties.

Even lower than those of their crystalline counterpart, the non linear properties of SBN epitaxial thin films are competitive with those of (Ba, Sr)TiO3 thin films for dielectric tunability and with those of crystalline $LiNbO_3$ for electro-optic properties.

7. References

Ahn, K.H. & Baih, S (2002). Change of growth orientation in Pt films epitaxially grown on MgO (001) substrates by sputtering. *Journal of Materials Research*, Vol. 17, No. 9 (September 2002), pp.2334-2338

Antsigin, V.D.; Egorov, V.M.; Kostsov, E.G.; Malinnovsky, V.K. & Sterelyukhina, L.N. (1985). Ferroelectric properties of thin strontium barium niobate films. *Ferroelectrics*, Vol. 63 (1985), pp. 235-242

Baginsky, I.L.; Gudaev, O.A.; Detinenko, V.A.;, Kostsov, E.G.; Malinovski, V.K.; Nesterikhin, Yu.E. & Pokrosky, L.D. (1978). Some peculiarities strontium barium niobate films and their electrophysical properties. *Ferroelectrics, Vol. 22 (1978, pp. 783-784.*

Boulay, N; Cuniot-Ponsard, M; Desvignes, J.M. & Bellemain (2007), A. Dielectric and ferroelectrics properties of $Sr_xBa_{1-x}Nb_2O_6$ (SBN: x) thin films. *Ferroelectrics,* Vol. 353 (2007), pp. 10-20.

Carruthers, J.R. & Grasso, M. (1970). Phase equilibria relations in the ternary system BaO-SrO-Nb_2O_5. *Journal of Electrochemical Society* Vol. 117, No. 11, (November 1970), pp. 1426-1430

Cuniot-Ponsard, M; Desvignes, J.M.; Ea-Kim, B & Leroy, E (2003a). Radio frequency magnetron sputtering deposition of hetero-epitaxial strontium barium niobate thin films ($Sr_xBa_{1-x}Nb_2O_6$). *Journal of Applied Physics*, Vol. 93, No.3, (February 2003), pp. 1718-1724.

Cuniot-Ponsard, M; Desvignes, J.M & Leroy, E (2003b). R. F. magnetron sputtering deposition of hetero-epitaxial $Sr_xBa_{1-x}Nb_2O_6$ thin films: the role of temperature. *Ferroelectrics*, Vol. 288, (2003), pp. 159-168.

Cuniot-Ponsard, M; Desvignes, J.M. & Bellemain,A (2006). Epitaxial growth of Sr_x Ba_{1-x} Nb_2 O_6 (SBN) thin films on Pt coated MgO substrates: the determining control of platinum crystallographic orientation. *Journal of Materials Science*, Vol. 41, (2006), pp. 5302-5309

Cuniot-Ponsard, M; Desvignes, J.M.; Bellemain, A & Bridou, F (2011). Simultaneous characterization of the electro-optic, converse-piezoelectric, and electro-absorptive effects in epitaxial (Sr, Ba)Nb_2O_6 (SBN) thin films.. *Journal of Applied Physics*, Vol. 109, 014107 (January 2011), pp. 1-11.

Francombe, M.H. (1960). . *Acta Cristallographica,* Vol. 13, (1960), pp. 131

Glass, A.M. (1969). Investigation of the electrical properties of $Sr_{1-x}Ba_xNb_2O_6$ with special reference to pyroelectric detection. *Journal of Applied Physics*, Vol. 40, No. 12, (November 1969), pp. 4699-4713

Guerra, J.de Los S.; Mendes, R.G. ; Eiras, J.A. ; Santos, I.A. & Araujo, E.B. (2008). Investigation of nonlinear dielectric properties in $Sr_{0.75}Ba_{0.25}Nb_2O_6$ relaxor ferroelectric thin films. *Journal of Applied Physics*, Vol.103 (2008), 014102, pp.1-8.

Jamieson; P.B.; Abrahams, S.C. & Bernstein, J.L. (1968). Ferroellectric tungsten bronze-type structures. I. Barium strontium niobate $Ba_{0.27}$ $Sr_{0.75}$ Nb_2 $O_{5.78}$. *The Journal of Chemical Physics,* Vol. 48, No. 11, (June 1968), pp. 5048-5057

Koo,J.; Jang, J.H.; Bae, B-S. (2000a). Optical and electrical properties of ferroelectric SBN thin films prepared by sol-gel process. *Journal of Sol-Gel Science and Technology,* Vol. 19, (2000), pp. 611-614

Koo,J.; Changho, L;Jang, J.H.; No, K. & Bae, B-S. (2000b). Measurement of the linear electro-optic coefficients of sol-gel derived strontium barium niobate thin films using a two beam polarization interferometer. *Applied Physics Letters,* Vol. 76, No. 19 (May 2000), pp. 2671-2673

Lairson, B.M.; Visokay, M.R; Sinclair, R; Hagstrom, S & Clemens, B.M. (1992). Epitaxial Pt(001), Pt(110), and Pt(111) films on MgO(001, MgO(110), MgO(111), and Al_2O_3(0001). *Applied Physics Letters* Vol. 61, No. 12 , (September 1992),pp. 1390-1392

Lenzo, P.V.; Spencer, E.G. & Ballman, A.A. (1967). Electro-optic coefficients of ferroelectric strontium barium niobate. *Applied Physics Letters,* Vol. 11, No. 1, (July 1967), pp. 23-24.

Li, X.T.; Du, P.Y.; Ye, H; Mak, C.L. & Wong, K.H. (2008). Electro-optic properties of epitaxial $Sr_{0.6}Ba_{0.4}Nb_2O_6$ filmsgrown on MgO substrates using $Li_xNi_{2-x}O$ buffer layer. *Applied Physics A,* Vol. 92 (2008), pp. 397-400.

Lin, W-J., Tseng, T-U.; Lin, S-P.; Tu, S-L.; Yang, S-J; Harn, J-J; Liu, K-S. & Lin, I-N. (1995). Growth of epitaxial-like ($Sr_{0.5}Ba_{0.5}$)Nb_2O_6 ferroelectric films. *Japanese Journal of Applied Physics,*Vol. 34 (1995), pp. L625-L627.

Lu, Z; Feigelson, R.K.; Route, R.K. ; Hiskes, R. & Dicarolis, S.A. (1994). Growth of (001)-oriented SBN thin films by solid source MOCVD. *Materials Research Society Proceedings,* Vol. 335 (1994), pp. 59-64

McIntyre, P.C.;Maggiore, C.J. & Nastasi, M (1995). Orientation selection in thin platinum films on (001) MgO. *Journal of Applied Physics,* Vol. 77, No. 12 (June 1995), pp. 6201-6204

McIntyre, P.C.;Maggiore, C.J. & Nastasi, M (1997). Epitaxy of Pt thin films on (001) MgO-I. Interface energetic and misfit accommodation. *Acta Materials,* Vol. 45, No. 2 (1997), pp. 869-878.

Moon S.E.; Kwak,M.H.; Kim, Y-T.; Ryu, H-C.; Lee, S-J. & Kang, K-Y. (2004). Measurement of microwave dielectric properties of (Sr, Ba) Nb_2O_6 thin films. *Integrated Ferrolectrics*, Vol. 66 (2004), pp. 275-281

Moon S.E.; Kwak,M.H.; Kim, Y-T.; Ryu, H-C.; Lee, S-J. & Kang, K-Y. (2005). Comparison of microwave performance for ferroelectric phase shifters based on (001) oriented (Ba, Sr) TiO_3 and (Sr, Ba) Nb_2O_6 thin films. *Journal of the Korean Physical* Society, Vol. 46, No. 1 (January 2005), pp. 273-276

Narayan, J; Tiwari, P; Jagannadham, K & Holland, O.W. (1994). Formation of epitaxial and textured platinum films on ceramics-(100) MgO single crystals by pulsed laser deposition. *Applied Physics Letters,* Vol. 64, No. 16 (April 1994), pp. 2093-2095

Nozaka, T.; Mizutani, Y.; Gun, B.; Echizen, M.; Nishida, T., Takeda, H.; Uchiyama, K. & Shiosaki, T. (2008). Effect of interface structure on electrical properties of (Ba, Sr)TiO_3 thin films on glazed alumina substrate. *Japanese Journal of Applied Physics,* Vol. 47, No. 9 (2008), pp. 7494-7499.

Sakamoto, W.; Yogo, T; Kikuta, K.; Ogiso, K; Kawase, A. & Hirano, S. (1996). Synthesis of strontium barium niobate thin films through metal alkoxide. *Journal of American Ceramic Society,* Vol.79, No. 9 (1996), pp. 2283-2288

Schwyn Thöny, S.: Youde, K.E., Harris, J.S., Hesselink, Jr. & L. (1994). Growth of epitaxial strontium barium niobate thin films by pulsed laser deposition. *Applied Physics Letters* Vol. 65, No. 16, (October 1994), pp. 2018-2020

Trivedi,D; Tayebati, P. & Tabat, M. (1996). Measurement of large electro-optic coefficients in thin films of strontium barium niobate ($Sr_{0.6}Ba_{0.4}Nb_2O_6$). *Applied Physics Letters,* Vol.68, No. 23 (June 1996),pp.3227-3229

Venturini, E.L.; Spencer, E.G.; Lenzo, P.V. & Ballman, A.A. (1968). Refractive indices of strontium barium niobate. *Journal of Applied Physics* Vol. 39, (1968), pp. 343-344

Willmott, P.R., Herger, R., Patterson, B.D., Windiks, R. (2005). Experimental and theoretical study of the strong dependence of the microstructural properties of $Sr_x Ba_{1-x} Nb_2 O_6$ thin films as function of their composition. *Physical Review B,* Vol. 71 (April 2005), 144114.

Zhang, H.Y.; He, X.H. & Shih, Y.H. (1991). A new method for measuring the electro-optic coefficients with higher sensitivity anf higher accuracy. *Optics Communications,* Vol. 86 (1991), pp. 509-512

Zhao, J; Li, Y; Liu, X;Zhang,H & Wang, B. (2004). Preparation and electrical properties of SBN thin films derived from aqueous organic gels. *Materials Letters*, Vol. 58 (2004), pp. 1456-1460

Zhu, L.D.; Zhao, J; Wang, F.; Norris, m95). Epitaxial electro-optical $Sr_xBa_{1-x}Nb_2O_6$ films by single source pasma-enhanced metalorganic chemical vapor deposition. *Applied Physics Letters,* Vol. 67, No. 13 (September 1995), pp. 1836-1838.

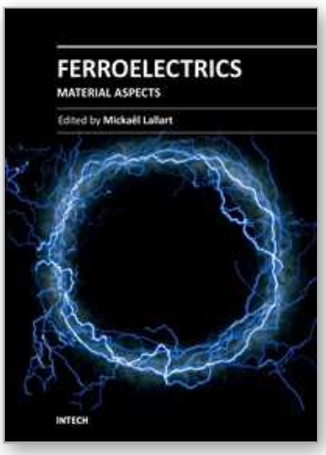

Ferroelectrics - Material Aspects

Edited by Dr. MickaÃ«l Lallart

ISBN 978-953-307-332-3
Hard cover, 518 pages
Publisher InTech
Published online 24, August, 2011
Published in print edition August, 2011

Ferroelectric materials have been and still are widely used in many applications, that have moved from sonar towards breakthrough technologies such as memories or optical devices. This book is a part of a four volume collection (covering material aspects, physical effects, characterization and modeling, and applications) and focuses on ways to obtain high-quality materials exhibiting large ferroelectric activity. The book covers the aspect of material synthesis and growth, doping and composites, lead-free devices, and thin film synthesis. The aim of this book is to provide an up-to-date review of recent scientific findings and recent advances in the field of ferroelectric materials, allowing a deep understanding of the material aspects of ferroelectricity.

How to reference

In order to correctly reference this scholarly work, feel free to copy and paste the following:

Mireille Cuniot-Ponsard (2011). Strontium Barium Niobate Thin Films for Dielectric and Electro-Optic Applications, Ferroelectrics - Material Aspects, Dr. MickaÃ«l Lallart (Ed.), ISBN: 978-953-307-332-3, InTech, Available from: http://www.intechopen.com/books/ferroelectrics-material-aspects/strontium-barium-niobate-thin-films-for-dielectric-and-electro-optic-applications

INTECH
open science | open minds

InTech Europe
University Campus STeP Ri
Slavka Krautzeka 83/A
51000 Rijeka, Croatia
Phone: +385 (51) 770 447
Fax: +385 (51) 686 166
www.intechopen.com

InTech China
Unit 405, Office Block, Hotel Equatorial Shanghai
No.65, Yan An Road (West), Shanghai, 200040, China
中国上海市延安西路65号上海国际贵都大饭店办公楼405单元
Phone: +86-21-62489820
Fax: +86-21-62489821

© 2011 The Author(s). Licensee IntechOpen. This chapter is distributed under the terms of the Creative Commons Attribution-NonCommercial-ShareAlike-3.0 License, which permits use, distribution and reproduction for non-commercial purposes, provided the original is properly cited and derivative works building on this content are distributed under the same license.

IntechOpen

IntechOpen